Avicenna Journal of Phytomedicine (AJP)

Original article

Enhanced bioavailability and cytotoxicity of disodium crocetinate over crocin in HCT-116 colorectal cancer cells: evidence from bioinformatics and experiments

Mahmoud Hassanpour[1], Mehran Ghaemi[2,3,*], Mahmoud Aminlari[1], Mohammad Reza Saberi[4], Salman AbdolahRamazani[4]

[1]*Department of Biochemistry, School of Veterinary Medicine, Shiraz University, Shiraz, Iran*
[2]*Department of Pathobiology, School of Veterinary Medicine, Shiraz University, Shiraz, Iran*
[3]*Department of Pathobiology, Faculty of Veterinary Medicine, Ferdowsi University of Mashhad, Mashhad, Iran*
[4]*Department of Medicinal Chemistry, School of Pharmacy, Mashhad University of Medical Sciences, Mashhad, Iran*

Article history:
Received: Mar 17, 2026
Received in revised form: May 29, 2026
Accepted: May 30, 2026
Epub ahead of print

**** Corresponding Author:***
Tel: +985138805631
Fax: +985138763852
m.ghaemi@um.ac.ir

Keywords:
Colorectal Neoplasms
Crocin
Crocetin
Disodium crocetinate
MMPs
ETV4
HCT-116 cells

Abstract

Objective: Colorectal cancer (CRC) remains a highly aggressive malignancy. This study directly compared the effects of crocin and disodium crocetinate (DSC) on human CRC HCT-116 cells.

Materials and methods: Crocin was converted to water-soluble DSC using alkali-catalyzed hydrolysis. Cells were treated with varying concentrations of crocin or DSC to assess viability. SYBR green quantitative real-time RT-PCR analyzed transcriptional modulation of matrix metalloproteinases 2 and 9 (*MMP-2* and *MMP-9*). Molecular docking with MOE software investigated binding modes of crocin and crocetin to the ETS translocation variant 4 (ETV4) protein.

Results: DSC induced a substantially stronger cytotoxic response than crocin, achieving an IC_{50} of 0.4 mM. In contrast, crocin did not reach 50% growth inhibition within the tested range, resulting in a non-experimentally measurable IC_{50} estimate of 3.3 mM. DSC treatment led to markedly greater downregulation of both *MMP2* and *MMP9* compared to crocin, consistent with prior work linking crocetin to inhibition of MAPK, NF-κB, and PI3K/Akt axes upstream of *MMP* transcription. Docking analysis revealed that crocetin physicochemical profile is vastly more aligned with ETV4 modulation.

Conclusion: Collectively, DSC constitutes a more potent inhibitor of CRC growth and metastatic potential than crocin, offering a mechanistically substantiated candidate for future preclinical evaluation. Crocin and crocetin act through ETV4 as a novel therapeutic target in the MAPK pathway.

Please cite this paper as:
Hassanpour M, Ghaemi M, Aminlari M, Saberi M.R, AbdolahRamazani S. Enhanced bioavailability and cytotoxicity of disodium crocetinate over crocin in HCT-116 colorectal cancer cells: evidence from bioinformatics and experiments. Avicenna J Phytomed, 2026

Introduction

Colorectal cancer (CRC) is a leading cause of cancer death and among the top three causes of cancer death worldwide; recent GLOBOCAN estimates report nearly two million new cases annually, with metastasis accounting for the majority of CRC-related deaths (Bray et al. 2024; Wu et al. 2025). Targeting key drivers of invasion is of paramount importance in improving patient outcomes.

Saffron (*Crocus sativus* L.) components – crocin, crocetin and safranal – have pleiotropic anticancer effects through antioxidant activity, suppression of nuclear factor kappa B (NF-κB) signaling, modulation of mitogen-activated protein kinase (MAPK) pathways and direct reduction of matrix metalloproteinases (MMPs) in various tumor types (Abdullaev 2002). Among natural bioactive compounds, crocin—a major carotenoid glycoside from saffron—has attracted much attention due to its antioxidant, anti-inflammatory, and anticancer activities (Bolhassani et al. 2014; Hasanpour et al. 2018; Mykhailenko et al. 2022). Crocin exhibits significant antiproliferative effects in several cancer cell lines including colorectal models, mainly through modulation of apoptosis-related pathways and inhibition of cell migration and angiogenesis (Bakshi 2022; Bakshi et al. 2022). Emerging evidence suggests that crocetin downregulates NF-κB signaling, reduces Reactive oxygen species (ROS)-dependent activation of *MMP* promoters, and interrupts phosphatidylinositol 3-kinase/ protein kinase B (PI3K/Akt) pathways—mechanisms intimately linked with CRC progression (Bahrami et al. 2024; Koch et al. 2024; Li et al. 2022; Zhou et al. 2025). Several *in vitro* studies have reported reduced expression and activity of MMP-2/9 after treatment with crocin or crocetin, supporting their anti-invasive potential (Bakshi et al. 2022; Zhuang et al. 2018).

Matrix metalloproteinases (MMPs) are zinc-dependent endopeptidases that remodel the extracellular matrix. MMP-2 and MMP-9 (gelatinases A and B) degrade type IV collagen and are involved in epithelial-to-mesenchymal transition, angiogenesis, and metastatic spread in CRC (Egeblad and Werb 2002; Overall and Kleifeld 2006). Elevated tumor or serum MMP-2/9 levels are associated with poor prognosis and increased metastatic potential (Wang et al. 2024). Accordingly, inhibition of MMP-2 and MMP-9 represents a valuable strategic therapeutic target, particularly for suppressing primary metastasis and modulating the invasive phenotypes of tumor cells. The pronounced clinical need to inhibit CRC cell invasion, together with growing evidence that crocetin derivatives potently regulate MMPs, makes a direct comparative study in HCT-116 cells critically important.

The therapeutic potential of crocin is significantly limited due to its poor bioavailability, low solubility, glycosylation level, and limited cellular uptake (Zeka et al. 2018). These pharmacokinetic obstacles necessitate the exploration of modified or derived forms of crocin with improved solubility, membrane permeability, and metabolic stability. Crocin undergoes enzymatic and acid hydrolysis to produce crocetin, its aglycone form, which exhibits superior lipophilicity and enhanced gastrointestinal absorption (Lautenschläger et al. 2015). However, crocin hydrolysis to crocetin is temperature- and time-dependent. According to a recent study, crocin is converted to crocetin in 20 min at 100°C (Shindo et al. 2022). Given the body temperature of about 37°C, crocin hydrolysis occurs less frequently and is mainly dependent on the gastric acid and intestinal enzymes, which potentiates unfavorable reactions and crocetin conjugated polyene core decomposition. The production of disodium crocetinate (DSC) from crocin is a practical chemical strategy to increase crocetin bioavailability while preserving biological activity, since DSC is more easily converted to crocetin in

acidic conditions than crocin. These provide a compelling mechanistic rationale for comparing crocin with its more bioavailable derivative, DSC, in CRC research (Figure 1).

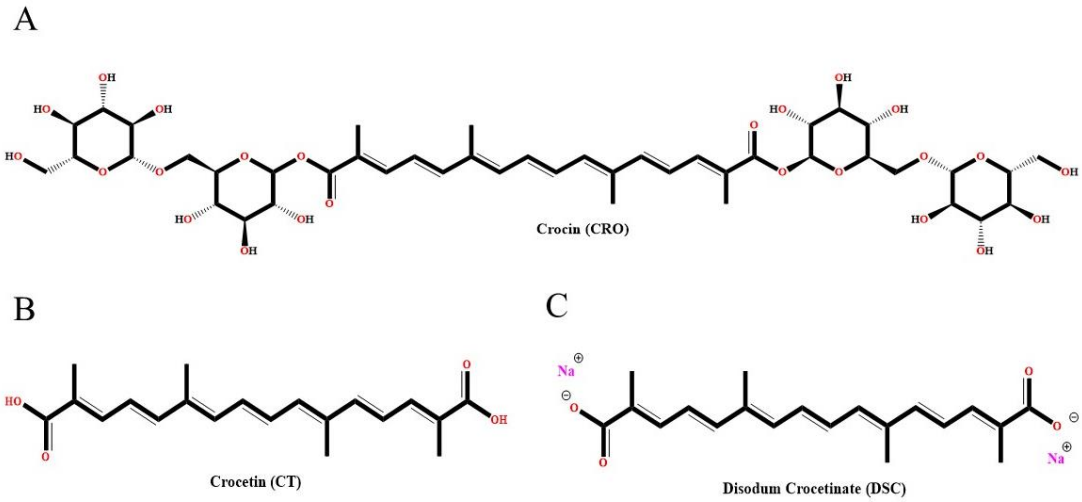

Figure 1. Chemical structures of crocin (A), crocetin (B) and disodium crocetinate (DSC) (C)

This study provides the first report on the impact of DSC on CRC cell lines, establishing a novel foundation for further research in this field. This study addresses an important gap in the current literature by establishing an optimized alkylation-based protocol for converting crocin to DSC, accompanied by rigorous physicochemical verification of the resulting compound, including solubility assessment and spectral characterization. In addition, the evidence specifically addressing DSC anticancer effects in cancers such as CRC remains scarce. Building upon this biochemical foundation, the investigation systematically evaluates both crocin and DSC in HCT-116 colorectal cancer cells through parallel analyses of cytotoxicity using the MTT assay and transcriptional regulation of metastasis-associated markers *MMP-2* and *MMP-9* via quantitative RT-PCR. We hypothesize that DSC also known as trans-sodium crocetinate will outperform crocin due to improved solubility and cellular availability, leading to stronger suppression of MMP-driven invasive pathways.

Materials and Methods

Materials and suppliers

Crocin (purity ≥95%) was obtained from Pooyesh Daru Sina Co. (Mashhad, Iran). The human colorectal carcinoma cell line HCT-116 was purchased from the Pasteur Institute of Iran (Tehran, Iran). Cell culture reagents, including RPMI-1640 medium, fetal bovine serum (FBS), penicillin–streptomycin, and trypsin-EDTA, were sourced from Gibco, Thermo Fisher Scientific (USA). MTT powder (purity ≥97%) was acquired from Sigma-Aldrich (St. Louis, MO, USA). Real-time PCR reagents, including RealQ Plus 2× Master Mix Green, were obtained from Ampliqon (Odense, Denmark). All oligonucleotide primers were synthesized by Metabion GmbH (Planegg, Germany). Analytical and molecular biology equipment included a Shimadzu UV–Vis spectrophotometer (Kyoto, Japan), a BioTek microplate reader (BioTek Instruments, Winooski, VT, USA), and a Corbett Rotor-Gene 6000 real-time PCR system (Qiagen, Hilden, Germany).

Methods

Synthesis and chemical conversion, spectroscopic confirmation and quality control of DSC

The stock solution of DSC was prepared through controlled alkaline hydrolysis of crocin. Specifically, crocin (5 mg) was first dissolved in warm deionized water (1 mL) to ensure complete solubilization. A dilute sodium hydroxide solution (0.01% w/v) was then added dropwise (4.2 mL total) under continuous stirring, and the reaction mixture was maintained in a 50°C water bath for 45 min at 100–200 rpm to promote conversion to DSC. Following incubation, the solution was allowed to cool to room temperature, and the pH was carefully adjusted to 7.4 using dilute hydrochloric acid (0.01% v/v). The final volume was brought to 5 mL with deionized water, yielding a stock solution with a theoretical concentration of approximately 1 mM DSC, assuming full conversion. The prepared solution was stored at −20 °C in light-protected tubes. Prior to each experiment, aliquots were thawed to room temperature, vortexed, gently mixed, and diluted to the required working concentrations immediately before use.

The chemical transformation of crocin into DSC was verified through visual observation and complementary physicochemical analyses designed to assess reaction completion, structural fidelity, and overall purity. Following hydrolysis and pH neutralization, aliquots of the reaction mixture were analyzed using UV–visible spectrophotometry (Shimadzu, Kyoto, Japan). Absorption scans were recorded from 200 to 750 nm and the predicted bathochromic shift in the λ_max characteristic was investigated.

Fourier-transform infrared (FTIR) spectroscopy was employed to further authenticate the chemical identity of the reaction product and to delineate the structural transitions associated with crocin deglycosylation and subsequent DSC formation. To enable direct comparison with the aglycone form and to validate the structural framework of the chromophore, crocetin was isolated from the DSC preparation via acidification-assisted extraction. Gradual addition of dilute hydrochloric acid lowered the pH to approximately 2–3, thereby protonating DSC and inducing the precipitation of poorly water-soluble crocetin. The orange–red precipitate was collected by centrifugation, washed with cold water to remove residual salts, and subsequently extracted with ethanol as a moderately polar organic solvent to selectively dissolve the carotenoid. Following solvent concentration under reduced pressure, the recovered crocetin served as a reference standard for spectral comparison.

Quality control assessments were conducted for every batch prior to experimental use. Stock solutions were visually inspected for turbidity, precipitation, or discoloration. The pH was routinely measured to ensure stability within the physiological range (pH 7.2–7.4), as deviations could indicate partial degradation or re-esterification.

Conversion of crocin and DSC to crocetin in simulated gastric condition

To assess the stability of crocin under gastric acidic conditions and to compare its behavior with that of DSC, 1 mM solutions of each compound were prepared following the alkalization procedure described in the Synthesis and Chemical Conversion section. Gastric acidity was simulated by the gradual addition of 0.12 M HCl to 2 ml of each solution until a final pH of 2 was reached. The total volume was then adjusted to 6 mL using deionized water. After gentle stirring to ensure homogeneity, approximately 2 mL of ethyl acetate was added to each sample. The mixtures were subsequently incubated in a shaking incubator at 100 rpm for 1 hr to facilitate phase interaction and compound extraction. Following incubation, the ethyl acetate phase was collected, and the amount of crocetin released into the organic layer was quantified spectrophotometrically. Crocetin solution was analyzed using UV–visible spectrophotometry. Absorption scans were recorded from 200 to 750 nm

and the predicted bathochromic shift in the λ_max characteristic was investigated. The amount of crocetin in each sample was quantified by drawing a standard graph.

Cell culture and treatment conditions

HCT-116 human colorectal carcinoma cells were cultured in RPMI-1640 medium supplemented with 10% fetal bovine serum, 100 U/mL penicillin, and 100 µg/mL streptomycin. Cultures were maintained at 37°C in a humidified atmosphere containing 5% CO_2. Cells were subcultured using 0.25% trypsin-EDTA once they reached approximately 70–80% confluence. To minimize phenotypic drift, only cell passages below 15 were used across all experiments.

For treatment studies, cells were seeded at assay-specific densities and allowed an attachment period of 24–48 hr. Subsequently, they were exposed to freshly prepared concentrations of crocin or DSC diluted in complete medium. Control groups received an identical volume of sterile deionized water.

MTT cell viability assay

Metabolic activity and cell viability were measured using the colorimetric MTT assay which measures the reduction of tetrazolium salt to insoluble formazan by mitochondrial dehydrogenases in metabolically active cells. HCT-116 cells were seeded in 96-well plates at a density of 5 to 8 × 10^3 cells per well and allowed to adhere and equilibrate for 48 hr under standard culture conditions. Following attachment, cells were treated for 24 hr with crocin or DSC at final concentrations of 0.06, 0.12, 0.25, 0.50, and 1.0 mM, each prepared freshly before administration to ensure maximal chemical stability and reproducibility. Control wells received an equivalent volume of deionized water. After exposure, the treatment medium was replaced with fresh medium, and then 10 µL of MTT stock solution (5 mg/mL in phosphate-buffered saline (PBS)) was added to each well. The plates were incubated for 3–4 hr at 37°C to allow formation of intracellular formazan crystals. After ensuring complete color conversion, the culture medium was carefully removed and, after drying, 100 µL of dimethyl sulfoxide (DMSO) was added to each well to solubilize the formazan product. Absorbance was recorded at 570 nm against blank, and background corrected at 630 nm using a BioTek microplate reader. Cell viability was calculated as a percentage of untreated control. Dose-response curves were generated and IC_{50} values were determined using nonlinear regression analysis (four-parameter logistic model) in GraphPad Prism. All measurements were performed in four technical replicates and repeated in at least three independent biological replicates to ensure reproducibility.

Primer design and validation

Primers targeting *MMP-2*, *MMP-9*, and the internal reference gene β2-microglobulin (*B2M*) were designed using NCBI Primer-BLAST under stringent, predefined parameters to ensure high analytical specificity and optimal amplification kinetics. The nucleotide sequences of the primers used were as follows: MMP2-F (5′ - TGGCAAGTACGGCTTCTGTC-3′) and MMP2-R (5′ - AGCTGTCATAGGATGTGCCC-3′) for *MMP-2* gene (PCR product of 110 bp), MMP9-F (5′ - CGGTTTGGAAACGCAGATGG-3′) and MMP9-R (5′- TGGGTGTAGAGTCTCTCGCT-3′) for *MMP-9* gene (PCR product of 176 bp), and B2M-F (5′ - AGGCTATCCAGCGTACTCCA-3′) and B2M-R (5′ - TGTCGGATGGATGAAACCCA-3′) for *B2M* gene (PCR product of 108 bp). Primer pairs were designed as intron spanning or exon-exon junction to prevent genomic DNA amplification in qRT-PCR. All primer pairs were synthesized by Metabion GmbH (Planegg, Germany).

Initial verification of primer specificity was performed by endpoint PCR followed by electrophoresis on 1.5% agarose gels, producing single, sharp amplicons of the expected molecular sizes without nonspecific bands. Amplification efficiency was determined using standard curves generated from a series of 5-fold cDNA dilutions; only primer sets exhibiting efficiencies of 90–110% and correlation coefficients ($R^2 \geq 0.99$) were selected for downstream quantitative analyses.

RNA extraction and quality assessment

Total RNA was extracted using the Denazist column RNA isolation kit (Iran) according to the manufacturer's guidelines. RNA concentration and purity were assessed spectrophotometrically using a NanoDrop instrument, ensuring A260/A280 ratios between 1.8 and 2.0. RNA integrity was further evaluated by electrophoresis on 1% agarose gels, which consistently revealed distinct 28S and 18S rRNA bands with minimal smearing, indicative of intact RNA suitable for high-fidelity downstream transcriptional analyses.

cDNA synthesis

First-strand cDNA was synthesized from 1 µg of total RNA using the Parstous cDNA synthesis kit (Iran), employing random hexamer primers in a final reaction volume of 20 µL. All reactions were performed alongside no-reverse-transcriptase (No–RT) controls. Completed cDNA samples were diluted and stored at −20°C until use in SYBR green real-time PCR assays.

SYBR green real-time qPCR

Quantitative expression analysis of *MMP-2*, *MMP-9*, and *B2M* was conducted using the Corbett Rotor-Gene 6000 real-time PCR system (Qiagen, Hilden, Germany). Each 20 µL reaction mixture contained: 10 µL Real Q Plus 2× Master Mix Green (Ampliqon, Denmark), 0.4 µL forward and reverse primers (10 µM), 2 µL diluted cDNA template and 7.2 µL nuclease-free water. Thermal cycling conditions were optimized for the selected primer sets and included; an initial denaturation at 95°C for 5 min followed by 94°C for 20 sec, 66°C for 20 sec, and 72°C for 15 sec, for 50 cycles.

Following amplification, high-resolution melting curve analysis (60–98°C) was performed to verify the presence of single, specific PCR products and to exclude primer–dimer artifacts. Gene expression levels were quantified using the ΔΔCt method, with *B2M* serving as the reference gene (Hu et al., 2023). All assays were conducted in technical triplicate, and inter-run calibrators were implemented to correct for plate-to-plate variability.

Mechanism of target discovery

In pursuit of a specific and therapeutically relevant protein target within the regulatory networks governing MMP-2 and MMP-9, we employed a systematic, pathway-centric bioinformatic strategy. Our analysis began with a detailed curation of the NF-κB, MAPK, and PI3K/AKT/mTOR (mTOR: mammalian target of rapamycin) pathways via the Reactome database (https://reactome.org), focusing on identifying key nodal proteins that functionally intersect these cascades upstream of MMP2/9 gene expression. This targeted review, supported by literature on MMP regulation in oncology, converged on the ETS (E-twenty-six) translocation variant 4 (ETV4) transcription factor as a compelling candidate. ETV4 emerged as a unique, non-redundant signaling hub, implicated in the transcriptional activation of some metastasis-promoting enzymes and the modulation of the MAPK pathways under investigation. Previous studies have demonstrated that ETV4 is involved in the main steps of organogenesis and is also a significant mediator of tumorigenesis and metastasis (Dumortier et al. 2018; Zhu et al. 2021). These findings are further supported by studies by Mathien et al. and other independent reports, which demonstrate

that *MMP* genes act downstream of the transcription factor ETV4 and are upregulated by ETV4 in lung and breast cancers (Bluestone et al. ; Mathien et al. 2015; Qin et al. 2008). Another study has revealed that ETV4 is among the most highly expressed genes in adenocarcinoma samples, based on an analysis of 689 differentially expressed genes between paired adenoma and adenocarcinoma tissues. *ETV4* inhibited by siRNA decrease of cell proliferation, colony formation and cell migration in the HT29 and SW480 colorectal cell lines (Fonseca et al. 2021).

Aforementioned, ETV4 is an important mediator in *MMPs* gene expression. Given the established therapeutic value of MMP-2 and MMP-9, we deployed an integrated computational pipeline to validate ETV4 as a novel target for the saffron bioactives crocin and crocetin.

Molecular docking

Molecular docking was performed using Molecular Operating Environment (MOE) software to investigate the binding modes of crocin and crocetin with the ETV4 protein. The three-dimensional structure of the human ETV4 receptor was retrieved from the RCSB Protein Data Bank (PDB ID: 5ILU) (PDB; http://www.rcsb.org/pdb/) (Currie et al. 2017; Kaffash et al. 2024). The chemical structures of the ligands, crocin and crocetin, were obtained from the PubChem database (Jafarisani et al. 2018). Prior to docking, all structures were prepared and energy-minimized using the Quick Prep tool within MOE. The docking procedure employed the London dG scoring function for initial placement, with the Triangle Matcher method generating ligand poses. These poses were subsequently refined and rescored using the GBVI/WSA dG scoring algorithm (Labute 2008; Vilar et al. 2008). To comprehensively identify potential binding sites, a blind docking approach was used, where the ligands were docked across the entire protein surface. The resulting pose with the most favorable (most negative) calculated binding free energy (ΔG, kcal/mol) for each ligand was selected for further analysis by molecular dynamics simulation.

Molecular dynamics (MD) simulation

MD simulations were conducted using the GROMACS software package to evaluate the stability and binding interactions of the selected ETV4-ligand complexes (Kaffash et al. 2024). Each system was constructed by placing the protein-ligand complex in a cubic simulation box with a 0.5 nm buffer distance from the box edges, which was then solvated with TIP3P (transferable intermolecular potential with 3 points) water molecules. As the ligands were electrically neutral, no additional ions were added for system neutralization (Kaffash et al. 2024). The systems underwent a two-step equilibration process: first under an NVT ensemble (constant Number of particles, Volume, and Temperature) for 100 ps, followed by an NPT ensemble (constant Number of particles, Pressure, and Temperature) for 100 ps, maintaining conditions of 300 K and 1 bar. Finally, a production MD simulation was run for 100 ns for each complex. The stability of the simulations was assessed by analyzing the root-mean-square deviation (RMSD) and root-mean-square fluctuation (RMSF) of the protein and the complexes.

ADMET properties (Absorption, distribution, metabolism, excretion and toxicity)

ADMET properties were predicted using the SwissADME and admetSAR web servers. Key descriptors, including LogP, molecular weight, and hydrogen bond counts, were calculated. Rule-based filters (Lipinski, Veber) assessed drug-likeness and oral bioavailability. Pharmacokinetic endpoints—absorption, distribution, metabolism, and excretion—were modeled. Toxicity risks, including mutagenicity and hepatotoxicity, were also evaluated computationally.

Statistical analysis

All experiments were performed using a minimum of three independent biological replicates. Statistical analyses were conducted using GraphPad Prism (version 10). Data distribution was assessed using the Shapiro–Wilk normality test.

Multiple group comparisons were analyzed using one-way analysis of variance (ANOVA) followed by Tukey's post hoc test.

Results are presented as mean ± standard deviation (SD), and differences were considered statistically significant at $p < 0.05$. Dose–response curves and IC_{50} estimates were generated by nonlinear regression using a four-parameter logistic model.

Results

Synthesis, chemical conversion, spectroscopic confirmation and quality control of DSC

Visual monitoring and reaction completion

Alkaline hydrolysis of crocin produced an immediate and distinguishable shift in solution color. The deep red appearance of the parent glycoside gradually transitioned to a lighter, more translucent red within the first 15–20 min, consistent with the formation of the crocetin dianion. No precipitate, turbidity, or particulate residues were observed during or after the reaction, indicating stable solubilization and uniform conversion.

UV–visible spectroscopic profiling

UV–Vis absorption scanning (200–750 nm) revealed a clear bathochromic displacement of the major carotenoid absorption band following hydrolysis (Figure 2 A). Crocin stock solution showed a λ_max at 443 nm, typical of glycosylated crocetin esters, and DSC demonstrated a shifted λ_max at 421 nm, consistent with full deglycosylation and formation of the disodium salt. Spectra showed no residual crocin shoulder peaks, confirming successful and complete conversion.

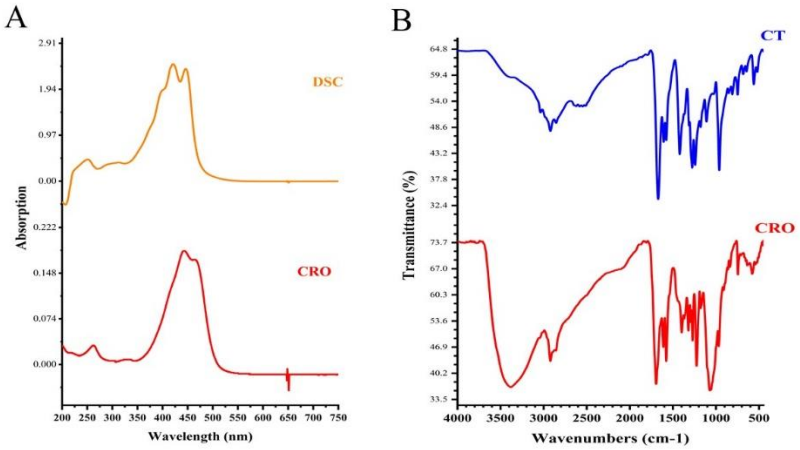

Figure 2. Spectroscopic characterization of crocin and disodium crocetinate (DSC). A) UV–Vis absorption spectra of crocin (▬) and DSC (▬). Crocin exhibited a characteristic λ_max at 443 nm, consistent with its di-gentiobiosylated structure, whereas DSC demonstrated the expected bathochromic shift to 421 nm, confirming complete alkaline hydrolysis and formation of the crocetin dianion. B) FTIR spectra of crocin and DSC. Crocin displayed ester C=O stretching near 1720–1735 cm^{-1} and glycosidic signatures, while DSC showed disappearance of ester bands characteristic of crocetin salts, along with preserved polyene chain vibrations (1500–1700 cm^{-1}). Together, these spectral transitions verify successful and high-purity conversion of crocin to DSC. CRO: crocin (▬), DSC: disodium crocetinate (▬) and CT: crocetin (▬).

FTIR-based structural authentication

Crocin and crocetin generally have similar FTIR spectra because they share the same carotenoid skeleton, but differ in key functional groups, and these differences provided a clear vibrational fingerprint that distinguishes crocin and isolated crocetin in FTIR.

Isolated crocetin, exhibited the expected carboxylic acid C=O peak at 1700 cm^{-1}, enabling direct structural validation (Figure 2 B).

The characteristic absorption bands of the conjugated polyene chain—typically observed within the 1500–1700 cm^{-1} region—along, provided a coherent spectral fingerprint confirming successful conversion to DSC (Figure 2).

Quality control of prepared stock solutions

All DSC stock preparations remained optically clear and free of precipitation throughout storage at −20°C. Immediately prior to use, pH was consistently within physiological range (7.2–7.4) for all batches.

Conversion of crocin and DSC to crocetin in simulated gastric condition

Visual inspection of the samples, supported by the data shown in Figure 3, revealed a clear difference between crocin and DSC under simulated gastric conditions. After 1 hr of incubation at pH 2, the ethyl acetate supernatant obtained from the crocin sample appeared noticeably paler than that of the DSC sample. This qualitative observation suggests limited hydrolysis of crocin under acidic conditions, consistent with the relative stability of its ester bonds. In contrast, the more intense coloration observed in the DSC supernatant indicates enhanced partitioning into the organic phase, reflecting a higher extent of conversion to crocetin.

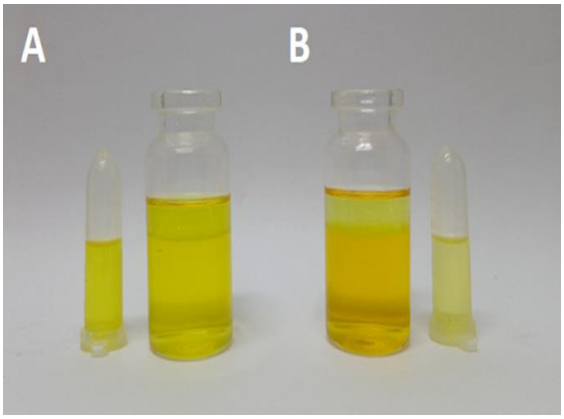

Figure 3. Visual observation of disodium crocetinate (DSC) solution (A) and crocin (B) under gastric acid conditions with pH 2 and temperature of 37°C at 100 rpm for 1 h. The purpose of adding the ethyl acetate supernatant solution is to measure the amount of crocetin extracted in the organic phase. Microtubes around each sample were removed from the ethyl acetate supernatant solution for visual identification, inspection, and spectrophotometric measurement. Disodium crocetinate exhibits significantly greater acid-mediated conversion to crocetin compared with crocin itself under simulated gastric conditions. This enhanced conversion may contribute to improved bioavailability and absorption of crocetin in the digestive tract.

To quantitatively confirm these observations, crocetin levels in the ethyl acetate phase were determined spectrophotometrically at a λ_max of 425 nm. Concentrations were calculated using the corresponding calibration curve derived from the linear absorbance–concentration relationship.

Effects of crocin and DSC on HCT-116 cell viability

Concentration-dependent reduction in metabolic activity

Exposure of HCT-116 cells to crocin or DSC for 24 hr resulted in a dose-dependent decrease in viability (Figure 4). DSC at concentrations ≥0.25 mM exhibited significant cytotoxic effects compared with the untreated control group ($p<0.0001$).

At the highest concentration tested (1 mM), DSC caused a significant decrease in viability (88.5%, $p<0.0001$) compared to crocin (25%). This indicates enhanced bioactivity following deglycosylation and salt formation.

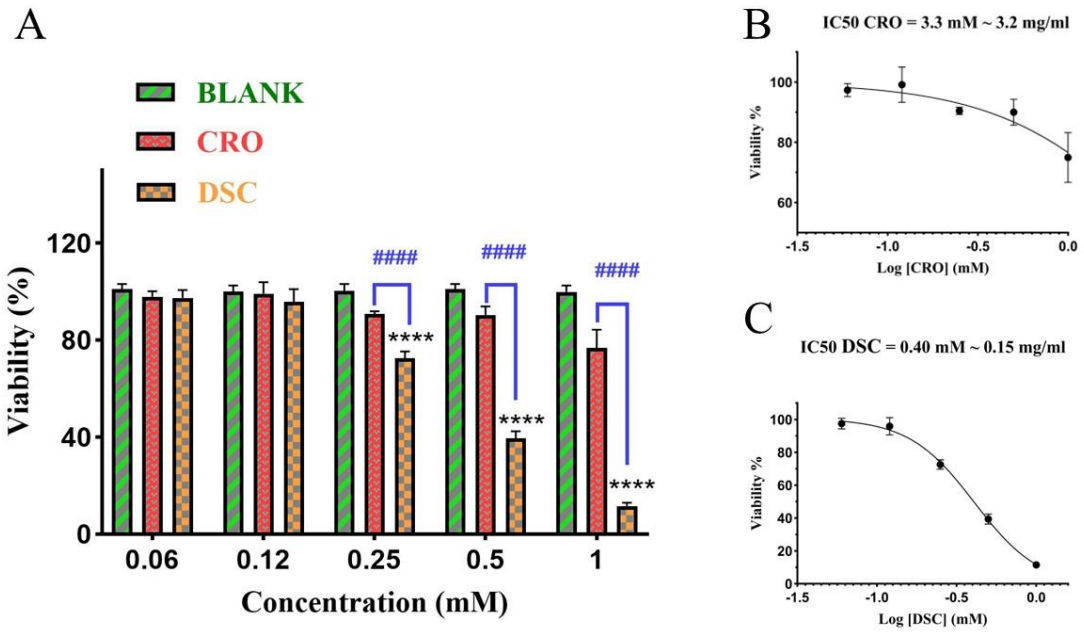

Figure 4. A) Comparative cytotoxic activity of crocin (CRO) and disodium crocetinate (DSC) in HCT-116 colorectal cancer cells. HCT-116 cells were exposed to matched concentrations of crocin or DSC (0.06, 0.12, 0.25, 0.50, and 1.0 mM) for 24 hr, and cell viability was quantified using the MTT assay. Data represent mean ± SD from three independent biological replicates (n = 3), expressed as percentage of untreated control (blank). Statistical significance was assessed by one-way ANOVA followed by Tukey's post hoc test. Crocin significantly reduced cell viability at 0.25, 0.50, and 1.0 mM (**p<0.01; ***p<0.001; and ****p<0.0001 vs. control). DSC elicited a markedly stronger cytotoxic response, showing highly significant reductions at 0.25, 0.50, and 1.0 mM (****p<0.0001 vs. control) and demonstrating superior potency compared with crocin at each corresponding dose (####p<0.0001 vs crocin). At the lower concentrations of 0.06 and 0.12 mM, no significant differences were observed among crocin and DSC, in comparison to the control group. B and C) Dose–response relationships of CRO and DSC in HCT-116 colorectal cancer cells following 24 hr of exposure. A definitive IC_{50} value was obtained for DSC, whereas crocin failed to reduce cell viability to 50% within the tested concentration range. Consequently, the IC_{50} for crocin could not be directly determined and was instead estimated by nonlinear regression using a normalized logarithmic inhibitory dose–response model.

IC_{50} determination

Nonlinear regression analysis using a four-parameter logistic model showed that crocin and DSC had markedly different IC_{50} values: 3.3 mM for crocin (though this value was not experimentally reached within the tested concentration range) and 0.4 mM for DSC.

DSC achieved a quantifiable IC_{50} within the tested concentration range, while crocin did not reduce cell viability less than 75% at the highest concentration (1.0 mM) and the IC_{50} was not reached experimentally. Dose-response analysis for crocin revealed a weak but concentration-dependent reduction in cell viability. However, viability did not decrease by 50% over the concentration range tested. So, the crocin IC_{50} value was determined by dose-response curve using nonlinear regression via a log [inhibitor] vs. normalized response by GraphPad Prism. Consequently, DSC showed an IC_{50} value approximately 8.5-fold lower than that of crocin, indicating a significant improvement in the HCT116 colorectal cancer cells cytotoxicity (Figure 4 B and C). Biological and technical replicates demonstrated robust reproducibility, with inter-experiment variability below 10%.

RNA integrity, cDNA quality, and primer performance

Total RNA isolated from control and treated HCT-116 colorectal carcinoma cells demonstrated excellent purity, with A260/A280 ratios consistently ranging

from 1.8 to 2.0. Agarose gel electrophoresis further confirmed RNA integrity, showing sharp, well-resolved 28S and 18S rRNA bands with minimal evidence of degradation. Reverse transcription produced high-quality cDNA suitable for quantitative expression analysis.

SYBR green qRT-PCR assay performance

All primer sets targeting *B2M*, *MMP-2*, and *MMP-9* exhibited strong and reproducible amplification efficiency. Reaction efficiencies fell within the optimal range of 104–110%, and all standard curves displayed high linearity (R^2 ≥0.92), confirming reliable quantification across the tested dynamic range. Melting curve analysis revealed single, well-defined peaks for each target 81°C (*B2M*), 85.8°C (*MMP-2*), and 90.3°C (*MMP-9*) indicating high specificity and the absence of nonspecific amplification or primer–dimer artifacts. Taken together, these parameters validate the analytical robustness of the qRT-PCR assays used in this study.

Importantly, all molecular analyses—including RNA integrity verification, high-efficiency cDNA synthesis, and qRT-PCR performance with efficiencies of 104–110% and sharp, single melting peaks—demonstrated methodological rigor, confirming that the observed fold-changes reflect true biological differences rather than technical variability.

Differential expression of *MMP-2* and *MMP-9*

Crocin and DSC suppress *MMP-2* expression

Both crocin and disodium crocetinate (DSC) significantly suppressed *MMP-2* gene expression in HCT-116 colorectal cancer cells compared with untreated controls. Exposure to crocin (0.32 mM) produced a modest yet statistically significant reduction in *MMP-2* mRNA levels (a 0.895-fold) relative to the control group (**p<0.05). Notably, treatment with DSC at the same concentration resulted in a far more pronounced downregulation, reducing *MMP-2* expression to a minimal fraction of control levels (0.039-fold of control, ****p<0.0001). Direct comparison between the two treatments further revealed that DSC mediated a significantly greater inhibitory effect on *MMP-2* transcription than crocin (####p<0.0001) (Figure 5).

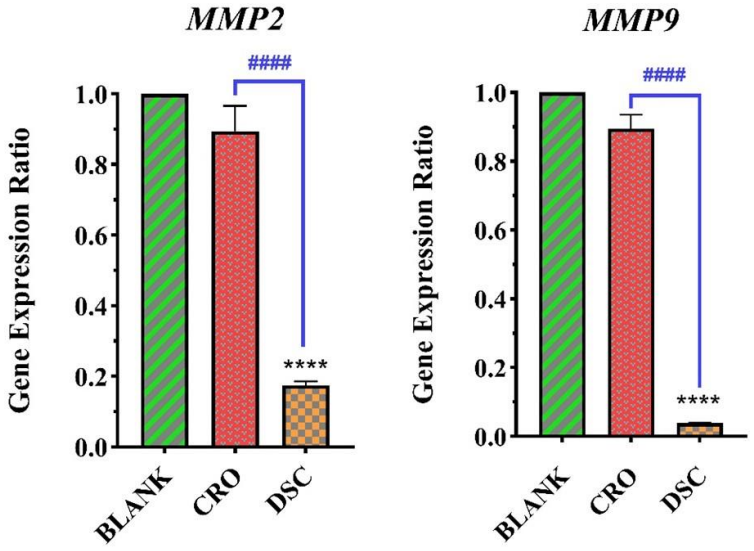

Figure 5. qRT-PCR analysis of *MMP-2*, *MMP-9* mRNA expression in HCT-116 human colorectal carcinoma cells after 24 hr of treatment with 0.32 mM crocin and DSC (disodium crocetinate). Treatment with crocin and DSC, significantly downregulated *MMP-2* and *MMP-9* transcription in HCT-116 cells. CRO (crocin), DSC (disodium crocetinate).

DSC exhibits potent inhibition of *MMP-9*

A similar pattern was observed for *MMP-9*, a key mediator of tumor invasion and metastasis. Crocin induced a moderate decrease in *MMP-9* expression (0.175-fold, $p<0.0001$). DSC again demonstrated superior efficacy, reducing *MMP-9* expression at the same concentration (0.087-fold of control, $p<0.0001$). Overall, DSC exhibited approximately twice the inhibitory strength of crocin toward *MMP-9* ($p<0.0001$), suggesting enhanced cellular accessibility or more efficient interference with upstream regulatory pathways controlling *MMP-9* transcription (Figure 5).

Comparative potencies

One-way ANOVA confirmed that DSC exerted significantly stronger inhibitory effects than crocin across both metalloproteinases ($p<0.0001$). These transcriptional differences align with cytotoxicity profiles obtained from MTT assays, further supporting the enhanced biological activity of DSC (Figure 5).

Docking results and binding mode analysis

Molecular docking successfully predicted the binding modes and affinities of crocin and crocetin within the ETV4 protein. The pose with the most favorable binding free energy (ΔG) for each compound was selected for further analysis.

Crocin demonstrated a binding energy of -8.5 ± 0.1 kcal/mol. Its structure fits within the ETV4 protein, with one glycosylated end fully embedded and the other end partially exposed. The interaction is stabilized by multiple residues including Arg387, Gln342, Trp381 and Tyr401 (Figure S1).

Crocetin exhibited a lower calculated binding affinity, with a ΔG of -5.8 ± 0.1 kcal/mol, however its more compact structure allowed for deeper and adopted engagement with the binding site, forming specific interactions with unique residues such as Ile407 and Ser429 (Figure 6).

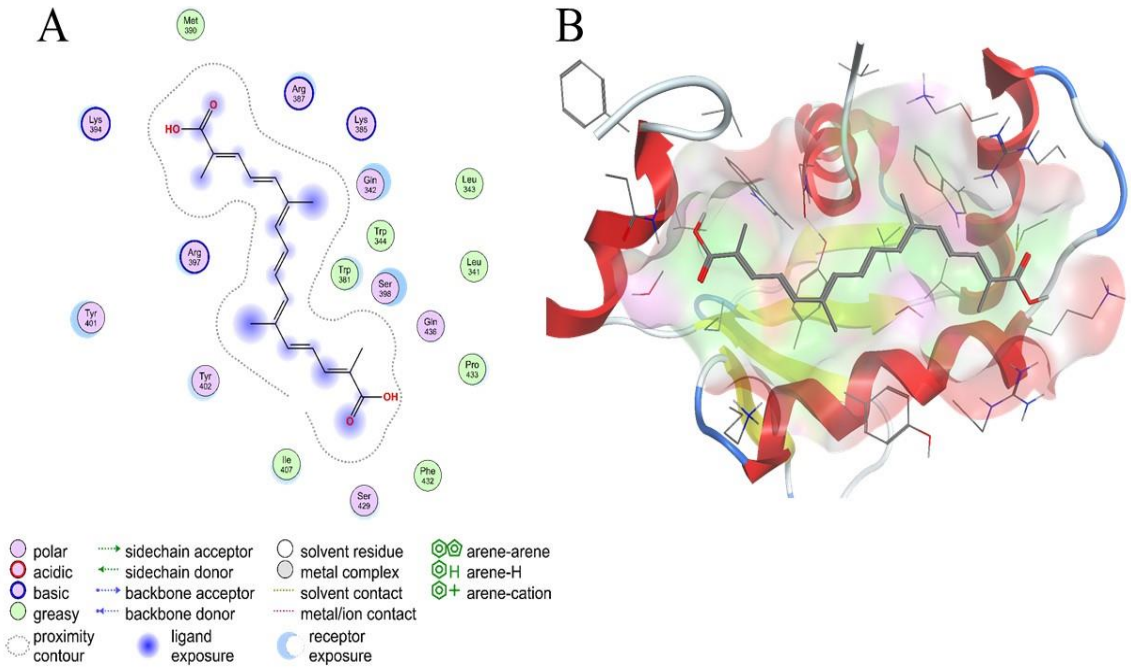

Figure 6. After molecular docking, ETV4 and crocetin interact. A) 2D structure, and B) 3D structure

A comparative analysis revealed a common binding region shared by both ligands. Key residues like Leu341, Leu343, and Phe432 contributed to this shared interaction network. Notably, Asp434 and Asn435 appeared to act as potential anti-binding factors for the shared region of the ligands, which may influence the overall binding energy profile. While Trp344 was in proximity to the central structure of both compounds, its direct role in stabilizing the complex remains unclear and may require further investigation (Figure S1 and Table S1).

Molecular dynamics simulation analysis

To validate the stability and persistence of the binding modes predicted by docking, 100-ns molecular dynamics (MD) simulations were performed on the ETV4-crocin and ETV4-crocetin complexes. The stability of each system was assessed by analyzing the root-mean-square deviation (RMSD) and root-mean-square fluctuation (RMSF).

Root-Mean-Square deviation (RMSD) analysis

The RMSD of the protein backbone was calculated to evaluate the overall structural stability and conformational convergence of the complexes throughout the simulation.

ETV4-Crocetin Complex Stability: The ETV4 backbone in complex with crocetin reached a stable equilibrium rapidly, with an average RMSD of approximately 1.8 Å over the final 80 ns of the simulation. This low and stable deviation indicates that the protein structure underwent minimal conformational rearrangement upon binding, suggesting a highly compatible and stable interaction (Figure 7A).

Ligand Positional Stability: The positional RMSD of crocetin relative to the protein binding site remained consistently low (average ~1.2 Å), confirming that the docked pose was maintained without significant dissociation or reorientation.

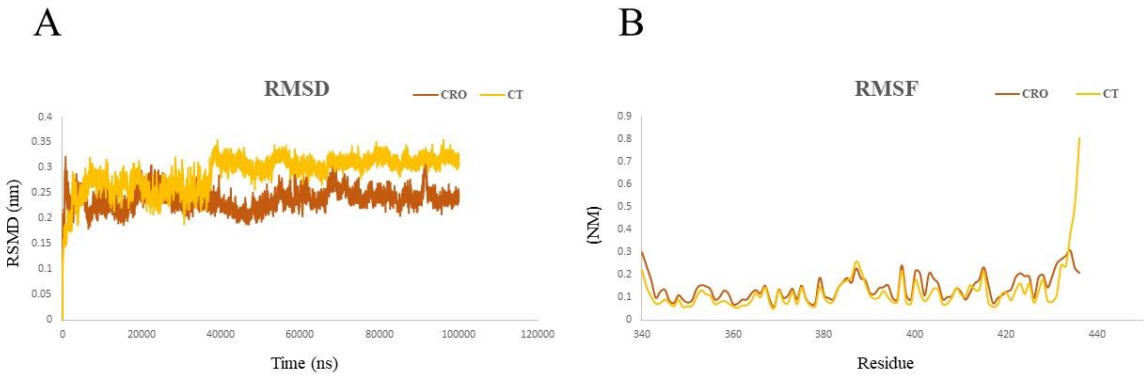

Figure 7. A) Diagrams of RMSD of ETV4 protein carbon-α in the presence of crocin and crocetin. B) Diagrams of ETV4 protein RMSF with Crocin and Crocetin are displayed.

Root-Mean-Square fluctuation (RMSF) analysis

The RMSF was computed to investigate the per-residue flexibility, particularly focusing on the binding site region identified in the docking studies.

Binding Site Rigidification: Residues forming the shared binding site (e.g. Leu341, Leu343, and Phe432) showed reduced flexibility (lower RMSF) in both complexes compared to the unbound ETV4 simulation, a characteristic sign of ligand-induced stabilization (Figure 7B).

Key Residue Behavior: Notably, Trp344—which was proximal to both ligands in the docking pose—displayed markedly reduced fluctuation in the crocetin complex. This suggests a stable interaction, potentially through π-stacking or hydrophobic contacts. Furthermore,

residues Asp434 and Asn435, hypothesized as potential anti-binding factors, showed distinct dynamics between the two complexes, which may partly explain the differential affinity (Figure 7).

Binding site conformation and interaction persistence

A visual analysis of the simulation trajectories confirmed the integrity of the binding site. For the ETV4-crocetin complex, the core hydrophobic interactions and key hydrogen bonds observed in the docking pose (e.g. with Ser429, Ile407) were maintained for over 85% of the simulation time. This persistent interaction network supports the higher affinity for crocetin (Table S2).

ADMET result

Crocin violated multiple drug-likeness rules due to its high molecular weight and polarity, predicting very poor intestinal absorption. In contrast, crocetin complied with key rules, showing favorable permeability and a high probability of oral bioavailability. Both compounds showed low predicted CNS penetration and were substrates for metabolic enzymes. Crocetin demonstrated a more favorable overall ADMET profile with no significant red flags for toxicity (Table 1).

Table 1. Summarizes the key comparative ADMET data.

Descriptor	Crocin (Cro)	Crocetin (CT)	Implication for CT
Molecular Weight	957.82 Da	328.41 Da	Far smaller, complying with standard drug-likeness rules.
LogP	2.44	4.61	Higher lipophilicity, suggesting better membrane permeability and potential oral bioavailability.
Rotatable Bonds	18	8	Markedly more rigid, leading to lower entropic penalty upon binding and more stable, predictable docking poses.
H-Bond Acceptors/ Donors	24/14	2/2	Drastically reduced polarity, improving passive diffusion and simplifying solvation models in simulation.
Surface Area	389.93 Å²	142.76 Å²	Compact size, enabling it to fit into deeper, more specific binding pockets on proteins like ETV4.

Discussion

This research develops an improved method to chemically convert crocin into DSC and confirms the resulting compound's properties through detailed analysis of its solubility and structure. Recognizing the limited existing data on DSC anticancer potential, particularly in CRC, the study then compares the effects of both crocin and DSC on HCT-116 cancer cells. It tests their cell-killing ability and measures their impact on the expression of two genes (*MMP-2* and *MMP-9*) linked to cancer spread. The central premise is that DSC's superior solubility will make it more effective than crocin at inhibiting the cellular pathways that drive invasion.

The comparative FTIR analysis of the purified compound against the starting material, crocin, provides definitive spectroscopic evidence for the successful chemical transformation to the target aglycone, crocetin. This interpretation is based on the critical disappearance of signature glycosidic bands and the concomitant emergence of functional group vibrations unique to the de-esterified, free acid product. The persistence of key absorbance bands in the regions of 2920–2850 cm^{-1} (alkyl C–H stretching) and 1600–1650 cm^{-1} (conjugated polyene C=C stretching) confirms the integrity of the carotenoid backbone throughout the synthetic sequence, establishing that the core chromophore remained intact during the conversion process. The most salient evidence for the structural modification, however, is found in two diagnostic spectral regions. Firstly, the characteristically broad

and intense hydroxyl stretch (3200–3600 cm^{-1}) attributed to the multi-hydroxyl sugar moieties of crocin is entirely absent in the product spectrum, replaced by a significantly weaker and narrower band consistent with the isolated carboxylic acid O-H of crocetin. Secondly, the complex ensemble of strong, overlapping C-O and C-O-C stretching vibrations (1000–1200 cm^{-1}), a direct fingerprint of the glycosidic ether and sugar alcohol linkages, is markedly diminished. Concurrently, the carbonyl region undergoes a decisive shift: the sharp ester C=O stretch of crocin at ~1740 cm^{-1} is replaced by a carbonyl signal at a lower wavenumber (~1705-1715 cm^{-1}), diagnostic of the hydrogen-bonded carboxylic acid functional group of crocetin. The collective spectroscopic profile—defined by the loss of polyol O-H and sugar C-O stretches, coupled with the characteristic downfield shift of the carbonyl absorbance—constitutes unambiguous verification that the glycosidic ester linkages were selectively cleaved. This yields the target aglycone structure, thereby confirming the successful chemical conversion from crocin to crocetin. This workflow provided a rigorous FTIR-based assessment of structural integrity and reaction completeness, enabling clear differentiation among crocin and crocetin (or DSC) based on their respective functional group together provided a robust chemical signatures and vibrational characteristics.

Through rigorous physicochemical confirmation—including the expected bathochromic shift to 421 nm and FTIR-defined loss of ester carbonyl features—our data confirm the successful structural conversion of crocin to DSC, a transformation that dramatically enhances aqueous solubility. These improvements in solubility and ionic character are likely central to DSC enhanced intracellular availability and align with previously reported bioavailability advantages of crocetin derivatives (Gainer et al. 2017).

The results of simulated gastric condition experiment showed that the concentration of crocetin extracted from the DSC sample was nine-fold higher than that obtained from the crocin sample under identical conditions. This substantial difference indicates that DSC undergoes more rapid and extensive conversion to crocetin in an acidic environment, thereby increasing its availability in a form that is more readily extractable into the organic phase. Collectively, these findings suggest that gastric acidity promotes the efficient conversion of DSC to crocetin, which may facilitate faster absorption within the acidic milieu of the gastrointestinal tract.

Just as trans-sodium crocetinate (TSC) can enhance the effects of crocin by improving its bioavailability, the conversion of crocin to water-soluble DSC - achieved through controlled alkylation and salt formation - will significantly increase cellular penetration, thereby enhancing its anticancer potency (Aminifard et al. 2024). DSC also acts as an oxygen diffusion enhancer, a property that improves the oxygenation of the tumor microenvironment and enhances the chemotherapeutic response in hypoxic cancer tissues (Shah et al. 2021; Wagner et al. 2000). In another study that investigated the bioavailability of crocetin by oral administration to rats, it was shown that crocetin is well absorbed and reaches its maximum plasma concentration in a short time of about 30 min after administration, with an excellent half-life of about 5 hr and an experimental bioavailability of 55 to 66% (Manhas et al. 2024). In another study, human gut microbiota facilitated conversion of crocin to crocetin and improved its absorption or bioavailability (García et al. 2024).

The present investigation provides compelling biochemical and molecular evidence that DSC, the alkaline-derived and water-soluble crocetin salt, exhibits substantially greater cytotoxicity potency than its parent compound crocin in HCT-116 colorectal cancer cells. Although

numerous studies have explored the anticancer properties of crocetin and related carotenoids, this is the first study to directly evaluate the effects of DSC on the proliferation and viability of colorectal cancer cells. The dramatic increase in cytotoxic activity—with DSC showing an IC_{50} roughly 8.5 times lower than crocin—demonstrates that deglycosylation and salt formation unlock the biological potential of crocetin-based molecules. The enhanced potency observed here is consistent with crocin well-documented pharmacokinetic limitations—including poor membrane permeability and extensive glycosylation—which hinder its intracellular accumulation (Zeka et al. 2018). In contrast, the small, lipophilic crocetin backbone readily traverses biological membranes, and its disodium salt form exhibits significantly improved dispersibility, explaining the greater metabolic disruption detected in MTT assays.

At the transcriptional level, both crocin and DSC significantly suppressed *MMP-2* and *MMP-9* expression, but DSC achieved a far more profound reduction, lowering transcript levels to approximately 10.5% and 96.1% of control, respectively. DSC acts as a transcriptional modulator of this metastasis-associated metalloproteinase. These collaginases are essential mediators of extracellular matrix degradation, epithelial–mesenchymal transition, angiogenesis, and metastatic dissemination in CRC (Egeblad and Werb 2002; Kessenbrock et al. 2010). The previous studies have shown saffron-derived compounds exhibit anti-metastatic and anti-invasive properties in various cancer models. For example, crocin has been reported to suppress *MMP-9* expression and cell invasion in gastric and breast cancer cell lines (Festuccia et al. 2014). In CRC models, crocin inhibits migration, invasion, and angiogenesis through suppression of TNF-α/NF-κB/VEGF (VEGF: vascular endothelial growth factor) signaling (Bakshi et al. 2022), while crocetin has demonstrated the ability to reduce proliferation and migration of HCT-116 cells via p38-MAPK activation (Khajeh et al. 2020).

Multiple prior studies have shown that crocetin derivatives implicated in the disruption of NF-κB, MAPK, PI3K/Akt, and ROS-dependent MMP transcriptional programs (Bakshi et al. 2022). Crocetin has been shown to inhibit NF-κB activation, reduce oxidative stress, and impair pro-inflammatory signaling, all of which converge on the regulatory elements controlling *MMP-2/9* promoters (Bhandari 2015; Premkumar et al. 2003).

crocetin and crocin, also exhibit antioxidant, anti-inflammatory, and anti-proliferative properties in cancer cell lines, suggesting additional mechanisms by which DSC or TSC as a synthetic and water-soluble derivative of crocetin may modulate cancer biology (Khajeh et al. 2020). preclinical studies in hypoxia-related disease models, including stroke, ischemia, and solid tumors, have demonstrated that TSC significantly increases tissue oxygenation and reverses hypoxia-induced signaling (Sheehan et al. 2009). In brain tumor models, tumor oxygenation was transiently elevated by TSC, thereby enhancing the response to radiotherapy (Sheehan et al. 2009). In other study have revealed TSC reduced intracellular ROS production and activated the phosphorylation of ERK (extracellular signal-regulated kinase) in HEK-293 cells. In addition, TSC decreased the levels of apoptosis and autophagy proteins (Rajabian et al. 2023). Liang et al have shown TSC in both animal model and cell culture effectively reversed hypoxia-induced biochemical abnormalities and reduced inflammatory cytokines, oxidative stress, and ROS accumulation. They also suggested TSC primarily targets the EGFR (epidermal growth factor receptor)/PI3K/AKT/NF-κB signaling axis (Liang et al. 2026).

In this study, both crocin and DSC reduced *MMP-2/9* expression in colon cancer cells, with DSC showing a much

stronger effect. The near-complete suppression achieved by DSC suggests that its anticancer activity goes beyond growth inhibition and includes the targeting of invasion-related pathways, likely due to more efficient cellular uptake and stronger interaction with upstream regulatory mechanisms.

Emerging evidence indicates that ETS transcription factors play important roles in tumor invasion and metastasis through regulation of matrix-degrading enzymes (Hollenhorst et al., 2011). Among these factors, ETS translocation variant 4 (ETV4), also known as Polyomavirus enhancer activator 3 (PEA3)/E1AF, has been reported to promote cancer progression by enhancing the transcription of genes involved in extracellular matrix remodeling and metastatic dissemination (Oh et al., 2012). Previous studies demonstrated that ETV4 can bind to ETS-responsive elements within the promoter regions of MMPs and stimulate their transcriptional activity (Kaya et al., 2016). In particular, elevated ETV4 expression has been associated with increased levels of MMP-2 and MMP-9, which are key mediators of extracellular matrix degradation, tumor invasion, and metastasis in colorectal and several other cancers (de Launoit et al., 2006; Aytes et al., 2013). Therefore, the observed reduction in *MMP-2* and *MMP-9* expression following treatment with crocin and DSC may be partially associated with modulation of upstream transcriptional regulators such as ETV4. Docking results and binding mode analysis suggest that while both compounds bind to an overlapping site on ETV4, according to Figure 6, and supplementary figure 1, crocetin is completely more suitable substrate in the active site of ETV4, while crocin cannot be suitable substrate in the active site due to its bulky sugar groups. Crocetin maintains a conserved orientation within the pocket, while Crocin displays orientation shifts associated with minor steric clashes and RMSD perturbation (Table 2, supplementary data). Finally, possible interaction between crocin/crocetin derivatives and ETV4 supports the hypothesis that these compounds may exert anti-metastatic effects through suppression of ETV4-mediated MMP regulation. However, further experimental studies are required to confirm the involvement of ETV4 in the anti-metastatic effects of crocin and crocetin/DSC and to elucidate the associated molecular pathways.

Together, these findings consolidate DSC as a highly optimized crocin derivative with superior solubility, bioavailability, and mechanistic efficacy. By substantially reducing viability and profoundly suppressing metastasis-associated proteases, DSC emerges as a promising candidate for preclinical development in CRC. These results also support broader applications of crocetin salt chemistry for improving the therapeutic performance of carotenoid-based natural products.

This study establishes DSC as a functionally enhanced and mechanistically potent derivative of crocin with significant cytotoxicity and anti-metastatic relevance in colorectal carcinoma. Controlled alkaline hydrolysis yielded a structurally validated, highly water-soluble DSC preparation that demonstrated dramatically improved cytotoxicity and robust suppression of the metastasis-driving enzymes MMP-2 and MMP-9. The nearly complete transcriptional inhibition achieved by DSC—far exceeding that of crocin—underscores its capacity to interfere with key regulatory pathways governing tumor invasion and extracellular matrix remodeling. Docking and molecular dynamics simulations confirmed that both crocin and crocetin interact with ETV4, crocetin possesses a significantly more favorable physicochemical profile for a potential lead. Its smaller size, greater rigidity (resulting in improved stability), and higher lipophilicity (leading to better bioavailability) account for this advantage.

In addition, our results have shown that DSC exhibits significantly greater acid-mediated conversion to crocetin compared with crocin itself under simulated gastric conditions. Therefore, crocetin emerges as the far superior candidate for further *in silico* investigation and subsequent *in vitro* validation as an ETV4 modulator. DSC therefore represents a promising candidate for further investigation in advanced preclinical models including migration and invasion assays, three-dimensional tumor models, *in vivo* metastasis studies, and comprehensive pharmacokinetic profiling. Its dual capacity to suppress proliferation and impede metastatic signaling highlights DSC potential as a next-generation, saffron-derived therapeutic agent for CRC. Collectively, these characteristics position DSC as a more effective and biologically relevant derivative for anti-metastatic and anti-proliferative CRC research.

Acknowledgment

This research was financially supported by grants from the Research Council of Shiraz University and using the facilities of the Faculty of Pharmacy, Mashhad University of Medical Sciences.

Conflicts of interest

The authors had no competing interests.

Funding

This study was supported by the Office of the Vice-Chancellor for Research, Shiraz University, Shiraz, Iran. This work is also part of a PhD thesis.

Ethical Considerations

All cell-based experiments were performed in accordance with the ethical guidelines approved by the Ethics Committee of Mashhad University of Medical Sciences (ethics code: IR.MUMS.REC.1400.233).

Code of Ethics

IR.MUMS.REC.1400.233

Authors' Contributions

M AL, M G, and MR S were supervisors and designed the work, revised it critically for important intellectual content, and approved the version to be published. M HP did the experiment, analyzed the data, managed the study, and wrote the manuscript. MR S provided the researchers with laboratories and instrumentation, designed the docking section of the paper, and validated its results. Data were analyzed and approved by S AR, M G, and M HP. S AR and M G helped in doing the research. All authors have read and approved the paper.

Abbreviations

Abbreviation	Full Term
ADMET	Absorption, Distribution, Metabolism, Excretion, and Toxicity
ANOVA	Analysis of Variance
B2M	Beta-2-Microglobulin
CRC	Colorectal Cancer
DMSO	Dimethyl Sulfoxide
DSC	Disodium Crocetinate
ECM	Extracellular Matrix
ETV4	ETS Translocation Variant 4
FBS	Fetal Bovine Serum
FTIR	Fourier-Transform Infrared Spectroscopy
GROMACS	GROningen MAchine for Chemical Simulations
MAPK	Mitogen-Activated Protein Kinase
MD	Molecular Dynamics
MMP	Matrix Metalloproteinase
MOE	Molecular Operating Environment
MTT	3-(4,5-Dimethylthiazol-2-yl)-2,5-Diphenyltetrazolium Bromide

Abbreviation	Full Term
NF-κB	Nuclear Factor Kappa B
NPT	Constant Number of Particles, Pressure, and Temperature
NVT	Constant Number of Particles, Volume, and Temperature
PBS	Phosphate-Buffered Saline
PDB	Protein Data Bank
PI3K	Phosphoinositide 3-Kinase
qRT-PCR	Quantitative Real-Time Polymerase Chain Reaction
RMSD	Root-Mean-Square Deviation
RMSF	Root-Mean-Square Fluctuation
ROS	Reactive Oxygen Species
SD	Standard Deviation
TIP3P	Transferable Intermolecular Potential with 3 Points

References

Abdullaev F.I (2002) Cancer chemopreventive and tumoricidal properties of saffron (Crocus sativus L.). EBM 227(1):20–5

Aminifard T, Mehri S, Rahbardar MG, Rajabian F, Rad AK, Hosseinzadeh H (2024) Trans-sodium crocetinate suppresses apoptotic and oxidative response following myoglobin-induced cytotoxicity in HEK-293 cells. IJBMS 27(6):768

Aytes A, Mitrofanova A, Lefebvre C, et al. Cross‐species regulatory network analysis identifies a synergistic interaction between FOXM1 and CENPF that drives prostate cancer malignancy. Cancer Cell 2014;25(5):638‐651

Bahrami A, Khalaji A, Bahri Najafi M, et al. (2024) NF-κB pathway and angiogenesis: insights into colorectal cancer development and therapeutic targets. Eur. J. Med. Res 29(1):610

Bakshi H (2022) Molecular analysis of the effects of crocin on acute myeloid leukaemia, pancreatic and colon cancer. Ulster University

Bakshi HA, Quinn GA, Nasef MM, et al. (2022) Crocin inhibits angiogenesis and metastasis in colon cancer via TNF-α/NF-kB/VEGF pathways. Cells 11(9):1502

Bhandari PR (2015) Crocus sativus L.(saffron) for cancer chemoprevention: a mini review. J tradit complement 5(2):81–87

Bolhassani A, Khavari A, Bathaie SZ (2014) Saffron and natural carotenoids: Biochemical activities and anti-tumor effects. BBA Reviews on Cancer 1845(1):20–30

Bray F, Laversanne M, Sung H, et al. (2024) Global cancer statistics 2022: GLOBOCAN estimates of incidence and mortality worldwide for 36 cancers in 185 countries. CA: Cancer J Clin 74(3):229–263

Currie SL, Lau DK, Doane JJ, et al. (2017) Structured and disordered regions cooperatively mediate DNA-binding autoinhibition of ETS factors ETV1, ETV4 and ETV5. Nucleic Acids Res 45(5):2223–2241

De Launoit Y, Baert JL, Chotteau‐Lelievre A, et al. The Ets transcription factors of the PEA3 group: transcriptional regulators in metastasis. BBA 2006;1766(1):79‐87

Dumortier M, Ladam F, Damour I, et al. (2018) ETV4 transcription factor and MMP13 metalloprotease are interplaying actors of breast tumorigenesis. BCR 20(1):73

Egeblad M, Werb Z (2002) New functions for the matrix metalloproteinases in cancer progression. Nat Rev Cancer 2(3):161–174

Festuccia C, Mancini A, Gravina GL, et al. (2014) Antitumor effects of saffron-derived carotenoids in prostate cancer cell models. Biomed Res Int 2014(1):135048

Fonseca AS, Ramão A, Bürger MC, et al. (2021) ETV4 plays a role on the primary events during the adenoma-adenocarcinoma progression in colorectal cancer. BMC cancer 21(1):207

Gainer JL, Sheehan JP, Larner JM, Jones DR (2017) Trans sodium crocetinate with temozolomide and radiation therapy for glioblastoma multiforme. J Neurosurg 126(2):460–466

García CJ, Beltrán D, Frutos-Lisón MD, García-Conesa MT, Tomás-Barberán FA, García-Villalba R (2024) New findings in the metabolism of the saffron

apocarotenoids, crocins and crocetin, by the human gut microbiota. Food Funct 15(18):9315–9329

Hasanpour M, Ashrafi M, Erjaee H, Nazifi S (2018) The effect of saffron aqueous extract on oxidative stress parameters and important biochemical enzymes in the testis of streptozotocin-induced diabetic rats. Physiol Pharmacol 22(1)

Hollenhorst PC, McIntosh LP, Graves BJ. Genomic and biochemical insights into the specificity of ETS transcription factors. Annu Rev Biochem 2011;80:437‑471

Hu, Y., Jiang, Q., Zhai, X., Liu, L., & Hong, Y. (2023). Screening and validation of the optimal panel of reference genes in colonic epithelium and relative cancer cell lines. Sci Rep 13(1), 17777.

Jafarisani M, Bathaie SZ, Mousavi MF (2018) Saffron carotenoids (crocin and crocetin) binding to human serum albumin as investigated by different spectroscopic methods and molecular docking. J Biomol Struct Dyn 36(7):1681–1690

Kaffash M, Tolou-Shikhzadeh-Yazdi S, Soleimani S, Hoseinpoor S, Saberi MR, Chamani J (2024) Spectroscopy and molecular simulation on the interaction of Nano-Kaempferol prepared by oil-in-water with two carrier proteins: an investigation of protein–protein interaction. Spectrochim. Acta - A: Mol Biomol 309:123815

Kaya M, Yoshida K, Higashino F, et al. ETS transcription factor ETV4 promotes metastasis of colorectal cancer through regulation of matrix metalloproteinases. Mol Cancer Res 2016;14(6):625‑634

Kessenbrock K, Plaks V, Werb Z (2010) Matrix metalloproteinases: regulators of the tumor microenvironment. Cell 141(1):52–67

Khajeh E, Rasmi Y, Kheradmand F, et al. (2020) Crocetin suppresses the growth and migration in HCT-116 human colorectal cancer cells by activating the p-38 MAPK signaling pathway. RPS 15(6):592–601

Koch W, Wawruszak A, Kukula-Koch W, et al. (2024) Exploring the therapeutic efficacy of crocetin in oncology: an evidence-based review. Naunyn-Schmiedeberg's Arch Pharmacol 397(3):1455–1476

Labute P (2008) The generalized Born/volume integral implicit solvent model: estimation of the free energy of hydration using London dispersion instead of atomic surface area. J Comput Chem 29(10):1693–1698

Lautenschläger M, Sendker J, Hüwel S, et al. (2015) Intestinal formation of trans-crocetin from saffron extract (Crocus sativus L.) and in vitro permeation through intestinal and blood brain barrier. Phytomedicine 22(1):36–44

Li S, Zhao C, Zhang C, Li J, Gao W (2022) Research progress of traditional Chinese medicine monomers in intervening colorectal cancer by regulating MAPK signaling pathway. Cancer Adv 5:e22014

Liang Q-H, Liu Q-Q, Tian S-Z, Yao Q-H, Ye X-Q, Liu W-C (2026) Dietary fucoidan supplementation ameliorates heat stress-induced liver injury in broilers via modulating peroxidation, lipid metabolism, and ferroptosis. Poult Sci 106489

National Center for Biotechnology Information (NCBI). PubChem database: Crocin; Crocetin. In: Available via PubChem database: Crocin; Crocetin https://pubchem.ncbi.nlm.nih.gov

Manhas D, Dhiman S, Kour H, et al. (2024) ADME/PK insights of crocetin: a molecule having an unusual chemical structure with druglike features. ACS omega 9(19):21494–21509

Mathien S, Meloche S, Moens U, Rothfels K, Seternes O, Soulez M (2015) p-S857 NCOA3:ETV4 bind MMP2 and MMP10 promoter In: European Bioinformatics Institute. https://reactome.org 2015

Mykhailenko O, Ivanauskas L, Bezruk I, Petrikaitė V, Georgiyants V (2022) Application of quality by design approach to the pharmaceutical development of anticancer crude extracts of crocus sativus perianth. Sci Pharm 90(1):19

Oh S, Shin S, Janknecht R. ETV1, 4 and 5: an oncogenic subfamily of ETS transcription factors. BBA 2012;1826(1):1‑12

Overall CM, Kleifeld O (2006) Validating matrix metalloproteinases as drug targets and anti-targets for cancer therapy. Nat Rev Cancer 6(3):227–239

Premkumar K, Abraham SK, Santhiya S, Ramesh A (2003) Protective effects of saffron (Crocus sativus Linn.) on genotoxins-induced oxidative stress in Swiss albino mice. Phytother Res 17(6):614–617

Qin L, Liao L, Redmond A, et al. (2008) The AIB1 oncogene promotes breast cancer metastasis by activation of PEA3-mediated matrix metalloproteinase 2 (MMP2) and MMP9 expression. MCB 28(19):5937–5950

Rajabian F, Mehri S, Razavi BM, Rad AK, Rahbardar MG, Hosseinzadeh H (2023) Effect of trans-sodium crocetinate on contrast-induced cytotoxicity in HEK-293 cells. IJBMS 26(2):148

Shah HM, Jain AS, Joshi SV, Kharkar PS (2021) Crocetin and related oxygen diffusion-enhancing compounds: Review of chemical synthesis, pharmacology, clinical development, and novel therapeutic applications. Drug Dev Res 82(7):883–895

Sheehan J, Sherman J, Cifarelli C, et al. (2009) Effect of trans sodium crocetinate on brain tumor oxgenation. J Neurosurg 111(2):226–229

Shindo K, Sakemi Y, Shimode S, et al. (2022) Changes of crocin and other crocetin glycosides in saffron through cooking models, and discovery of rare crocetin glycosides in the yellow flowers of freesia hybrida. Front nutr 9:885412

Vilar S, Cozza G, Moro S (2008) Medicinal chemistry and the molecular operating environment (MOE): application of QSAR and molecular docking to drug discovery. Curr Top Med Chem 8(18):1555–1572

Wagner PD, Hsia CC, Goel R, Fay JM, Wagner HE, Johnson Jr RL (2000) Effects of crocetin on pulmonary gas exchange in foxhounds during hypoxic exercise. J Appl Physiol 89(1):235–241

Wang Y, Wei Y, Huang J, et al. (2024) Prognostic value of matrix metalloproteinase-2 protein and matrix metalloproteinase-9 protein in colorectal cancer: a meta-analysis. BMC cancer 24(1):1065

Wu S, Zhang Y, Lin Z, Wei M (2025) Global burden of colorectal cancer in 2022 and projections to 2050: incidence and mortality estimates from GLOBOCAN. BMC cancer 25(1):1770

Zeka K, Ruparelia KC, Sansone C, Macchiarelli G, Continenza MA, Arroo RR (2018) New hydrogels enriched with antioxidants from saffron crocus can find applications in wound treatment and/or beautification. Skin Pharmacol Physiol 31(2):95–98

Zhou L, Zhang J, Zhao K, Chen B, Sun Z (2025) Natural products modulating MAPK for CRC treatment: A promising strategy. Front pharmacol 16:1514486

Zhu T, Zheng J, Zhuo W, et al. (2021) ETV4 promotes breast cancer cell stemness by activating glycolysis and CXCR4-mediated sonic Hedgehog signaling. Cell Death Discov 7(1):126

Zhuang X, Dong A, Wang R, Shi A (2018) Crocetin treatment inhibits proliferation of colon cancer cells through down-regulation of genes involved in the inflammation. Saudi J Biol Sci 25(8):1767–1771

Supplementary

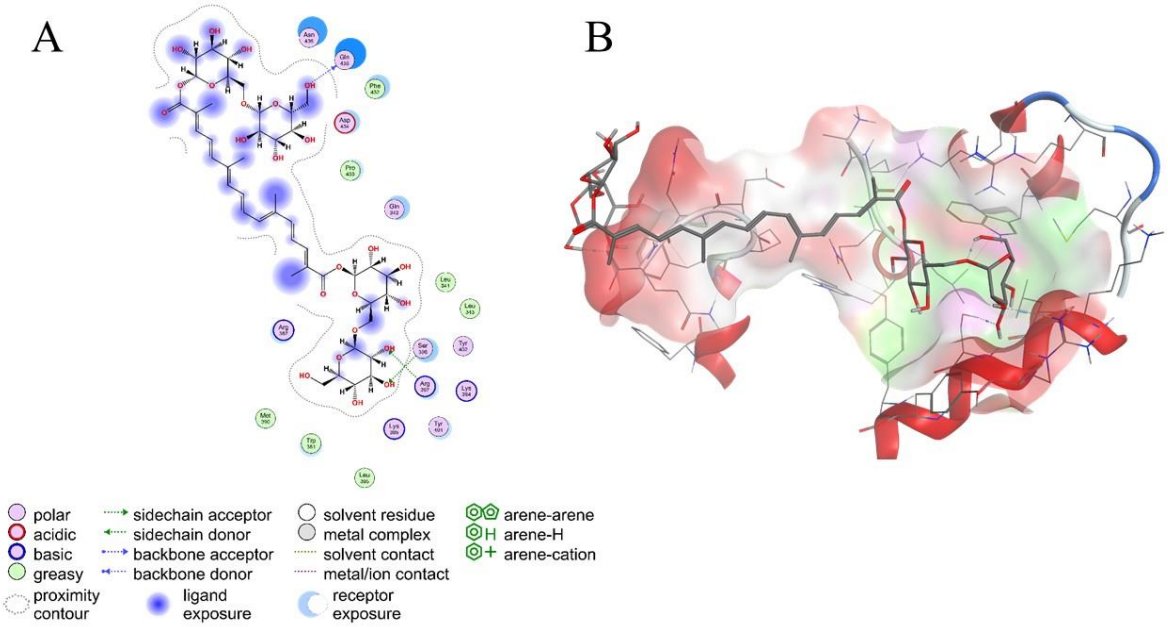

Supplementary Figure 1. After molecular docking, ETV4 and Crocin interact. A) 2D structure, and B) 3D structure.

Supplementary Table 1. Summarizes the key docking results

Compound	**Binding Energy (Δg, Kcal/Mol)**	**Shared Binding Residues**	**Unique Binding Residues**
Crocin	-8.52 ± 0.1	Arg387, Arg397, Gln342, Gln436, Leu341, Leu343, Lys385,	Asn435, Asp434, Leu395
Crocetin	-5.81 ± 0.1	Lys394, Met390, Phe432, Pro433, Ser398, Trp381, Tyr401, Tyr402	Ile407, Ser429, Trp344

Supplementary Table 2. Summary of Key MD Simulation Metrics for ETV4-Ligand Complexes

Complex	**Avg. Protein Backbone RMSD (Å)**	**Key Stable Interactions (Occupancy >80%)**
ETV4-Crocetin	1.8 ± 0.2	Hydrophobic core (Phe432, Leu343); H-bonds with Ser429
ETV4-Crocin	2.5 ± 0.4	Intermittent H-bonds with Arg387, Gln342; sugar moiety solvation